Progress In Electromagnetics Research B, Vol. 15, 217–244, 2009

CHARACTERIZATION AND MITIGATION OF RANGE ESTIMATION ERRORS FOR AN RTT-BASED IEEE 802.11 INDOOR LOCATION SYSTEM

J. Prieto Tejedor, A. Bahillo Martinez and S. Mazuelas Franco

CEDETEL (Center for the Development of Telecommunications of Castilla y León)
Edificio Solar, Parque Tecnológico de Boecillo
47151, Boecillo (Valladolid), Spain

R. M. Lorenzo Toledo, P. Fernández Reguero, and E. J. Abril

Department of Signal Theory and Communications and Telematic Engineering
University of Valladolid, Campus Miguel Delibes
Camino del Cementerio s/n, 47011, Valladolid, Spain

Abstract—Inaccurate range estimates often restrict indoor positioning systems, resulting in a more remarkable drawback when using an already-deployed IEEE 802.11 network. This is the case of the time delay based location system that this paper deals with. The main causes of these inaccuracies are multipath and non-line-of-sight (NLOS) effects. These effects can be solved to a large degree by characterizing arrival times and range estimation errors. For this reason, this paper analyzes multipath and NLOS effects involved in the round-trip time (RTT) discrete measuring process, which is conducted before each range estimate. RTT observations obtained in this process for different real indoor environments provide useful statistical information that allows to make the work extendable to other similar scenarios. Moreover, from this statistical information, the nodes in the network can estimate several parameters of the range estimates distribution while performing the location process. These are used to reduce the error caused by multipath components and to predict and correct the NLOS biases produced. In this way, the NLOS error is dynamically estimated and corrected, achieving better results than classical approaches based on static parameters.

Corresponding author: J. Prieto (jprieto@cedetel.es).

1. INTRODUCTION

In the recent past, global navigation satellite system (GNSS) has changed for the better, with more signals, more satellites, and better accuracy and integrity, all helping to open up new applications and possibilities for the future [1–3]. However, the indoor environment still remains nearly inaccessible for this system. In a parallel way, WLAN technologies are likely to become more important than they have ever been before as users and manufacturers find, in this environment, new scenarios where positioning, navigation and timing information are useful to them, and where GNSS cannot meet their needs [4]. Whichever the technology is used, indoor device location is a challenging research topic mainly due to multipath fading and non line-of-sight (NLOS) propagation errors [5–7]. Hence, a key issue in the design of a location system in this environment is measurements and error characterization [8].

This paper analyzes the results of time of arrival (TOA) measurements campaign performed at 2.4 GHz in a real indoor environment, using an already-deployed IEEE 802.11 network. TOA systems have a serious problem in installing and maintaining hardware for synchronization. However, the use of a round-trip time (RTT) method removes the time synchronization requirement. In this paper, the system utilized is a hardware estimator of the RTT between two wireless nodes, a mobile user (MU) and an access point (AP), which exchange several pairs of request-to-send (RTS) and clear-to-send (CTS) frames [9]. In [10] this system was used to estimate the location of an MU along an indoor route, with known fixed position of several APs. In spite of the presence of a line-of-sight (LOS) path between the MU and the AP, multipath components (MPC) alter the point estimation, generating an observed delay profile (ODP) which depends on the propagation channel and whose characterization will improve the resulting distance estimation [11, 12].

Therefore, the first goal is to find an appropriate distribution function for the description of RTT measurements. The most widespread model in literature for characterizing the arrival times is the Δ-K model [13]. Nevertheless, only a few references address the issue of modeling arrival times at 2.4 GHz in indoor scenarios, probably due to the difficulty of obtaining accurate TOA measurements with conventional WLAN devices. In [14], a discrete-time version of the Δ-K model is used to characterize the path arrivals from a measurement campaign at 2.4 GHz and 5.8 GHz in a real underground mine. However, the resulting propagation characteristics significantly differ from those frequently encountered in

more typical indoor environments. In this paper, the Δ-K model and a nonhomogeneous Poisson process (NHPP) are analyzed for modeling the RTT measurements.

RTT characterization allows to reduce the bias and the error in distance estimation. As commonly adopted, this error obeys a Gaussian distribution when the MU and the AP are in LOS [15]. This feature is contrasted with actual estimations taken by the mentioned RTT measuring system.

Apart from MPC distortion, if NLOS error is introduced, the resulting distribution will be the sum of the previous Gaussian error and another NLOS error frequently treated as Gaussian, Exponential, Weibull or Gamma [15–17]. The Exponential distribution is the simplest of these models, since it has only one unknown parameter. Thus, in this paper, it is selected to characterize the NLOS error, and a method for dynamically estimating its rate parameter is proposed. In this way, NLOS error can be partially reduced through the prior NLOS measurements correction method (PNMC) [16] which will focus on the last part of the paper. As the final goal is to include this work in a real-time application, the dynamic computation of PNMC input arguments, rate parameter and window size will improve the final distance estimation. Once again, this is corroborated through actual measurements.

2. RTT MEASURING SYSTEM

This section makes a brief description of the RTT-based positioning implementation carried out in [10] to locate an MU in an indoor environment. The obtained RTT measurements can be modeled as a discrete linear time-invariant (LTI) system whose response is studied as well. The empirical result of this system is analyzed in the next section.

2.1. Location Scheme

The hardware system described in [9] was used together with the IEEE 802.11b RTS/CTS mechanism to measure the RTT. This system consists of a printed circuit board (PCB) including a 16-bit clock cycles counter which is activated by the departure of an RTS frame from the WLAN adapter of the MU and stopped by the arrival of the corresponding CTS response from the AP. The signals which stamp these times are located on two leads of the MU's baseband processor, and they are clock synchronized, operating at 44 MHz. Therefore, the theoretical maximum accuracy is 6.8 m, which matches up with the

range resolution for an IEEE 802.11b network [18]. However, several statistical estimators and a simple linear regression model were assessed in [19] in order to improve the discrete time resolution.

A driver interacts with the PCB through the PC Parallel Port. The flowchart in Fig. 1 illustrates the steps that have been performed on the driver to obtain the MU position. Briefly, the general stages are:

- *Measure received signal strength (RSS)*: The MU WLAN adapter detects nearby APs by beacon signals that transmit every 100 ms.
- *AP MAC Filter*: The driver selects only the APs whose position is known. If there are at least 3 APs or more (needed for trilateration in two dimensions), the driver goes on to the next step.
- *Measure RTT*: In this stage, the system obtains the RTT to each AP in range through several sub-processes, which are detailed in the right of Fig. 1. This will allow computing the distance between the MU and each AP, storing it in a database.
- *Trilateration*: This process uses the databases *Distance Estimations* and *AP Positions* as inputs to estimate the MU location. The *Trilateration* technique is based on the radical axis of the circles centered at each AP position whose radii will be the estimated distances [10].
- *Print MU position*: the MU position is updated after each loop.

On the other hand, the right plane of Fig. 1 describes the child flowchart of the *Measure RTT* stage. It depicts the specific processes which this paper will deal with in depth. First, the driver selects the AP with the highest signal strength, sending RTS frames until the number of frames injected ($NPKT$) exceeds the minimum needed ($n_{\min}$) to guarantee a given confidence level. Simultaneously to the RTS last bit departure, the system counter is activated, and it will be stopped with the corresponding CTS arrival, saving the LOS and NLOS RTT measurements ($RTTs_{NLOS}$). Next, the scale parameter of the Weibull distribution (WS) is used to obtain a single RTT value (RTT_{NLOS}). This RTT value is the independent variable in a simple linear regression model whose result is the desired distance estimation [19]. Depending on the environment characteristics, this estimation will be distorted by NLOS error [20]. Therefore, this error is corrected through the PNMC method which is based on a statistical processing of a record of range estimates taken over a time window [16]. Afterwards, the driver connects to the next AP in terms of signal strength and the whole *Measure RTT* process is repeated.

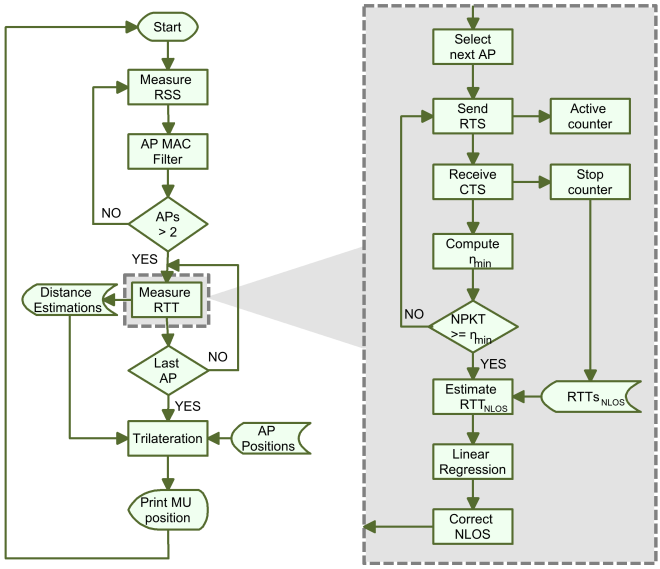

Figure 1. Flowchart for PCB main program driver. $NPKT$ = number of RTS frames injected, $n_{\min}$ = minimum number of RTS frames needed, $RTTs_{NLOS}$ = RTT measurements affected by NLOS error, RTT_{NLOS} = single value for the RTT after computing the WS of $RTTs_{NLOS}$.

2.2. Discrete Time LTI System

In Fig. 2(a) the three frequency stages of the classical heterodyne MU adapter are illustrated for both directions, transmission and reception, together with three blocks: two of them representing RTS and CTS propagation channels ($h(t)$ and $h'(t)$) and a black box symbolizing the AP. For the same distance and the same environment the channel impulse responses (CIR), $h(t)$ and $h'(t)$, are modeled as LTI systems. Different MPCs will alter the value of $h(t)$ and $h'(t)$ which will be detailed in the next section. These MPCs and the rest of the mentioned blocks will influence the impulse response of the discrete RTT measuring system.

As shown in the discrete-time blocks in Fig. 2(a) (PCB and $h''[n]$), initial and final timestamps are generated at baseband processor in RTS transmission and CTS reception respectively. Thus, grouping the RTS timestamps together (generated at times n_i in Fig. 2(b)), they

can be expressed as an impulse train:

$$s[n] = \sum_{i=1}^{N} \delta[n - n_i] \tag{1}$$

being N the total number of RTT measurements. Assuming that none of the frames is lost, and grouping the CTS timestamps together (ODP in Fig. 2), the response to $s[n]$ can be defined by:

$$r[n] = \sum_{i=1}^{N} \delta[n - n_i'']. \tag{2}$$

With this RTT measuring system, time windows in the upper part of Fig. 2(b) are never overlapped. Therefore, assuming all the transmitted impulses generated at the initial time, n_0, as in the bottom of Fig. 2(b), $s[n]$ and $r[n]$ can be rewritten as:

$$s[n] = N\delta[n] \tag{3}$$

$$r[n] = \sum_{j=1}^{M} F\left[j\Delta\right] \delta\left[n - j\Delta\right] \tag{4}$$

where M is the number of different bins of width Δ and $F[n]$ the frequency of occurrence, i.e., the number of received samples at each bin, thus $N = \sum_{j=1}^{M} F[j\Delta]$. In (4), $j\Delta$ represents in some way the discrete multipath delay. Therefore, when the propagation channel does not vary, the measuring system can be treated as a discrete-time

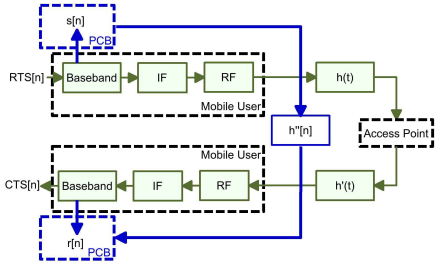

(a) Block diagram of the MU-AP communication (continuous-time blocks) and of the RTT measuring system (discrete-time blocks).

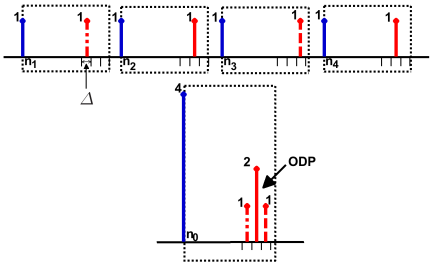

(b) Discrete time LTI response.

Figure 2. Discrete time LTI system and its impulse response.

LTI system, whose impulse response is:

$$h''[n] = \sum_{j=1}^{M} w[j\Delta]\delta[n - j\Delta] \tag{5}$$

where $w[n]$ is the relative frequency of each bin, i.e., $w[n] = F[n]/N$. In this way, when the channel is constant, the ODP can be obtained by convolution ($r[n] = s[n] * h''[n]$). In the next section, $w[n]$ is modeled as the intensity function, $\lambda(t)$, of an NHPP where t is discretized in bins of duration Δ.

3. MODELING THE RTT

This section first outlines the experimental setup of the RTT measuring process conducted in [9] and [19] and certain general aspects observed in the measurements behavior. After that, channel characteristics, which cause the deviation from the actual RTT, will be described together with their influence in the measurements (i.e., in the stored values in the database $RTTs_{NLOS}$ in Fig. 1). All of this, will help to investigate the statistical behavior of the RTTs.

3.1. RTT Measurements

In order to analyze the RTTs when the MU and the AP are in LOS situation, the first RTT measuring campaign was performed in an outdoor environment, with few street lamps within a 40 meter radius. MU and AP were located guaranteeing the first Fresnel zone clearance, conducting three series of 5000 samples for 15 distances between 0 and 40 m. Commercial Linksys WRT54GL IEEE 802.11b/g AP was selected whose reference clock has a frequency of 20 MHz and which includes two rubber duck omnidirectional antennas in diversity mode, working with the one with better reception. Antennas provide vertical polarization with 360 degrees of coverage in the horizontal plane and 75 degrees in the vertical one. The MU WLAN adapter is a Cisco Aironet AIR-PCM340 IEEE 802.11b card with the Intersil HFA3861B baseband processor working at 44 MHz. This WLAN adapter includes two on-board patch antennas with a diversity switch which toggles to and from and stops when a significant amount of RF power is detected.

ODP for distances 0, 8 and 35 meters is shown in Fig. 3. The binwidth (Δ) used to plot the histogram is 2 clock cycles (45.45 ns). This value is selected because, using one clock cycle, there is a large spike approximately every other clock cycle, and a less significant one in the rest, so statistical nature of the dataset would be hidden. This

behavior is caused by the frequency difference between MU and AP's clocks.

As a consequence of implementing the location system in a real scenario, incoming traffic from other networks and signal multipath will induce noise in distance estimations. Moreover, shot and thermal noise, as well as manufacturing and semiconductor defects of electronic devices, will cause signal disturbances even being the MU and the AP still and in LOS situation. These will be other sources of error in measuring the RTT. As seen in Fig. 3, identical distribution is appreciated if measurements are carried out at the same distance, i.e., at the same propagation channel. Thus, the RTT measurements distribution changes among the three subfigures are mainly due to propagation channel changes (while slight time deviations are caused by electronic errors). Besides, in Fig. 3, the NHPP and Δ-K model fits are very close, which is due to the independence of the RTT measurements, corroborated in [10]. These fits will be detailed in the last part of this section. Therefore, in the following, RTT measurements will be treated as independent and identically distributed (i.i.d.) observations.

3.2. Multipath Components in the Propagation Channel

In Fig. 3, RTT measurements do not consist of a single delta delayed a fixed RTT. This is due to electronic behavior and propagation channel structure and composition. Even in LOS situation, the receiver's measured signal represents a constructive or destructive summation of individual MPCs due to several scatterers [7]. Thus, the CIR can be represented by an LTI filter as:

$$h(t) = \sum_{n=1}^{R} A_n \delta(t - \tau_n) \tag{6}$$

where A_n is the amplitude of the nth MPC, τ_n its arrival excess delay, and R the total number of MPCs whose amplitudes exceed the detection threshold [21].

In Fig. 3, the symmetry of the ODP is affected, being the mass of the distribution concentrated on the right (negative skew) as the number of MPCs is higher, like Fig. 3(c), and in contrast, measurements exhibit the opposite behavior when there are fewer MPCs, as in Fig. 3(a). Therefore, the skewness (i.e., the asymmetry) can be a measurement of the degree of multipath being more negative as multipath is more noticeable. Moreover, considering all the distances, an inverse dependence is observable between distance and skewness, i.e., the more distance the more negative the skewness.

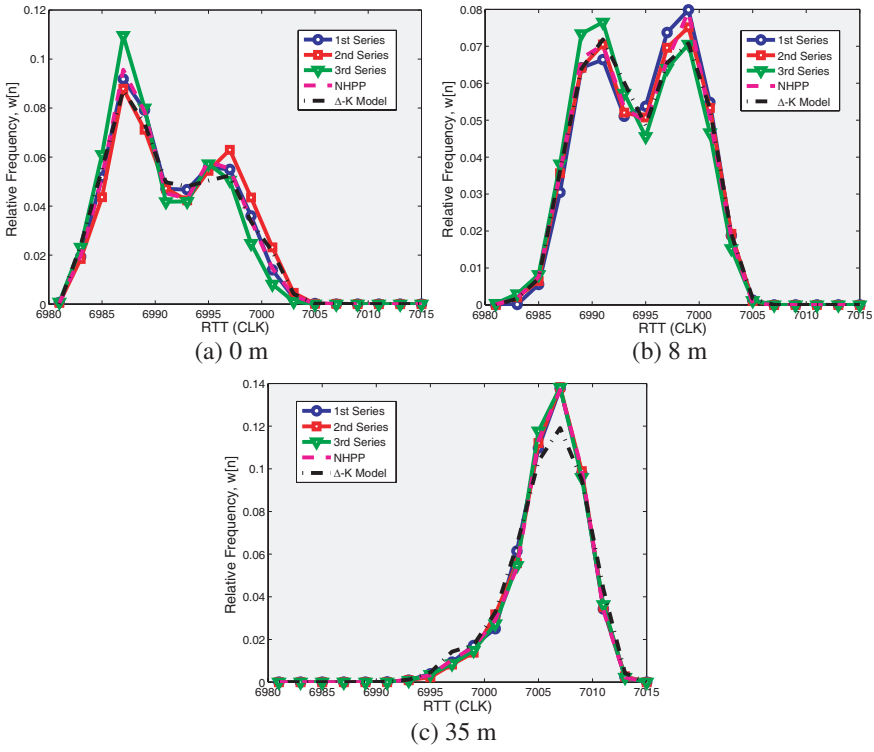

Figure 3. Three series of RTT measurements obtained in the LOS scenario for three different distances. Besides, NHPP and Δ-K model fits are shown (Section 4).

The latter means that longer signal paths are finally reflected before completing the round-trip. This is due to the fact that, when MU and AP are close enough, a greater number of signals follow the direct path (since small angles are insignificant), but when MU and AP are more distant, narrow angles are more noticeable, and most of the signals reflect on the ground.

Also, from Fig. 3, kurtosis (i.e., the degree of peakedness) tends to be greater as distance is larger since direct and ground-reflected paths tend to be the same length. This is trivial since the height of the MU and the AP is constant, thus, the segment MU-AP (direct path) tends to be the same length as the sum of the segments MU-G and G-AP (reflected path), being G the reflection point on the ground. Similarly, [21] proposed a NLOS identification technique based on the kurtosis and two statistics of the delay of the received MPCs in an UWB channel. However, with this technique several series of

measurements at each position and to each AP have to be conducted to obtain the distribution of these statistics, in order to compare them to the LOS/NLOS channel models. This is not feasible in a real-time application. Future work could be addressed to estimate the degree of multipath from the skewness and kurtosis of one series of measurements (the one needed for estimating the RTT) at each position, whereas NLOS would be detected and corrected with the PNMC method.

3.3. RTT Distribution

MPCs cause that the RTT follows a statistical pattern which depends on the propagation channel even in LOS scenarios. Thus, although electronic errors were negligible, a signal in transit from transmitter to receiver would undergo multipath dispersion due to reflections, refractions, and scattering from nearby objects or walls [7]. Hence, arrival times form a point process on the positive time axis. Several point process models have been discussed in the literature for the distribution of path arrival times for wireless urban [13, 22] or indoor environments [23, 24], where inadequacy of the homogeneous Poisson process (HPP) model has been proved. They all agree by fitting the arrival time sequences to a modified Poisson distribution. Here, two models have been considered to fit the RTT measurements (i.e., the relative frequency, $w[n]$), the Δ-K model and an NHPP.

3.3.1. The Δ-K Model

Standard Poisson distribution should only be appropriate if the obstacles which cause MPC appearance are located with complete randomness in space, a good assumption for homogeneous urban areas, but not in indoor scenarios where clusters of scatterers are commonly present (and therefore isolated clusters of reflected signals arrive at the receiver) [22, 23]. The most widespread model in mentioned publications is the Δ-K model, first proposed by Turin et al. [13]. Two possible states for a bin i of duration Δ are considered: $X_i = 0$, which indicates no path in the bin; and $X_i = 1$ that signifies a path in the bin. The model is based on the conditional probabilities of change of state. In this way, $\{\lambda_i\}$ and $\{K_i\}$ are defined as $P(X_i = 1|_{X_{i-1}=0}) = \lambda_i$ and $P(X_i = 1|_{X_{i-1}=1}) = K_i\lambda_i$. In this case, the duration of each bin is selected to be 2 clock cycles ($\Delta \approx 45.45\,\text{ns}$). In Fig. 3, Δ-K model shows a good fit to the RTT measurements with the PCB. However, λ_i and $K_i\lambda_i$ exhibit a similar distribution, since RTT measurements are i.i.d. Thus, although λ_i and $K_i\lambda_i$ are conditional probabilities, the probability of event X_{i-1} occurring does not affect the probability of event X_i occurring. For $K = 1$ or $\Delta = 0$ and constant $\lambda(t)$, this process

Table 1. P-value resulting from the two-samples KS test comparing NHPP or Δ-K models to empirical samples.

		0 m		8 m		35 m	
		NHPP	Δ-K	NHPP	Δ-K	NHPP	Δ-K
P-value	1st Series	0.8055	0.2752	0.0693	0.0397	0.8370	0.0208
	2nd Series	$4.4 \cdot 10^{-4}$	$7.8 \cdot 10^{-4}$	0.9994	0.9999	0.9630	0.0240
	3rd Series	$4.8 \cdot 10^{-7}$	$8.3 \cdot 10^{-12}$	0.0707	$4.2 \cdot 10^{-4}$	0.9883	0.0026

reverts to an HPP [22]. When arrival times are i.i.d. random variables, the standard (and stationary) Poisson hypothesis should be adequate. However, RTTs do not show a constant $\lambda(t)$. The explanation is that — with the described PCB — clusters of paths are not detected, storing only the time for the first arrival, leaving out multipath dispersion not involved in this measure. In order to develop useful statistical multipath channel models, it is imperative to determine the average number of MPCs and the distributions about the average [25], not possible with the PCB since it has to wait for a CTS response to start another count. For insensitive receivers the Poisson fit should be relatively good [23].

3.3.2. Nonhomogeneous Poisson

For systems whose rate, $\lambda(t)$, varies with time, as in Fig. 3, an NHPP is often used as model. An NHPP is a generalization of an HPP, and the rate at which events occur is determined by the intensity function $\lambda(t)$ [26]. The intensity function is assumed to be nonnegative for all $t \in (0, M\Delta]$, with M a known constant. For the RTT measurements the cumulative intensity function is defined by:

$$\Lambda(t) = \int_0^t \lambda(\tau) d\tau, \ t > 0 \tag{7}$$

and it can be used to generate a point process for simulation by inversion.

Figure 3 illustrated the probability of path occupancy for each delay time bin, Δ, of 2 clock cycles for the Δ-K model and the NHPP. This probability distribution depends on propagation channel characteristics. Thus, it has to be modeled each time the channel changes. Both models provide a high goodness of fit (GOF) to WLAN fading data. A good Δ-K model fit is probably due to the fact that this distribution has two parameters, increasing the flexibility to match the empirical data. However, K is close to 1, so NHPP, with $\lambda(t)$ as intensity function, provides a similar fit to the data (NHPP is

equivalent to Δ-K model with $K = 1$). Actually, in Table 1, P-values resulting from the two-samples Kolmogorov-Smirnov (KS) test, comparing NHPP or Δ-K models to each series of empirical samples, are shown. Better results for the NHPP model are obtained with a high GOF (P-value $\geqslant 0.05$) for almost all the series of measurements.

4. CHARACTERISTICS OF RANGE ESTIMATES

RTT characterization allows to reduce the bias and the error in the database *Distance Estimations* in Fig. 1. *Estimate* RTT_{NLOS} and *Linear Regression* processes will explain how to obtain these estimations in case RTT measurements are carried out in an LOS scenario. Afterwards, the estimation error is analyzed, assuming LOS between the MU and the AP (thus, *Correct NLOS* process is not included). Based on this result, the process *Compute* $n_{\min}$ will be detailed searching for a reduction in the number of frames injected in the WLAN network. Finally, the analysis of the error distribution will be performed generalizing for the NLOS case. Once the NLOS error is characterized, this work is used in the next section to correct it.

4.1. Distance Estimation

As seen in the previous section, RTT characterization is not an easy task. Therefore, it is necessary to select the statistical estimator which best approximates the RTT from the measurements conducted by the PCB, as they are affected by different sources of errors. It was analyzed in depth in [19], selecting the WS as the best estimator (see Appendix A for further information). In Fig. 1, the block *Estimate* RTT_{NLOS} reflected this process.

As explained in Fig. 1, after obtaining a single value for the RTT, a simple *Linear Regression* is performed to obtain an estimation of the distance between the MU and each AP in terms of meters. Table 2 contains the analysis of variance for the simple linear regression model for the measurements of previous section, taking 50 range estimates at each one of the 15 distances [27]. The description column shows the source of variation of each row which contain: the sum of squares (SS), its associated degrees of freedom (df), and the ratio of these or the mean square ($MS = \frac{SS}{df}$). Last column contains the F-ratio, which is the ratio of the regression mean square to the residual mean square. It follows that this ratio is distributed as Snedecor's-F with 1 and $T - 2$ degrees of freedom, T being the number of treatments ($T = 50 \cdot 15$). A test with significance level α for the null hypothesis is given by rejecting H_0 if $F > F_{\alpha;1,T-2}$. Rather than comparing F with

$F_{\alpha;1,T-2}$ for a specified value of α, a common practice is to assess the P-value for the test of the hypothesis of zero slope. The hypothesis is rejected at level α if $P(F > F_{\alpha;1,T-2}) < \alpha$. In this case, $F = 17250$, the P-value is close to zero.

Table 2 also includes the coefficient of determination (R-squared), defined as the ratio of the regression sum of squares to the corrected total sum of squares. R-squared is commonly used as an indicator of the proportion of the total variation in the response (distance) that is accounted for by variation in the input variable (RTT estimation). Both the F-test and R-squared provide evidence that WS is a useful predictor. Note that R-squared is made without regard to sample size whereas the F-test takes this into account in the degrees of freedom. However, the long sample size allows to assess the GOF with both indicators [27].

4.2. LOS Scenario

In LOS scenarios, distance estimation can be expressed as a function of the actual distance d_i adding an error for the j treatment at that

Table 2. Analysis of variance for linear regression data.

Description	*df*	*SS*	*MS*	*F*
Regression	1	98240	98240	17250
Residual	748	4260	5.6951	
Total	749	102500	136.8	$R^2 = 0.958$

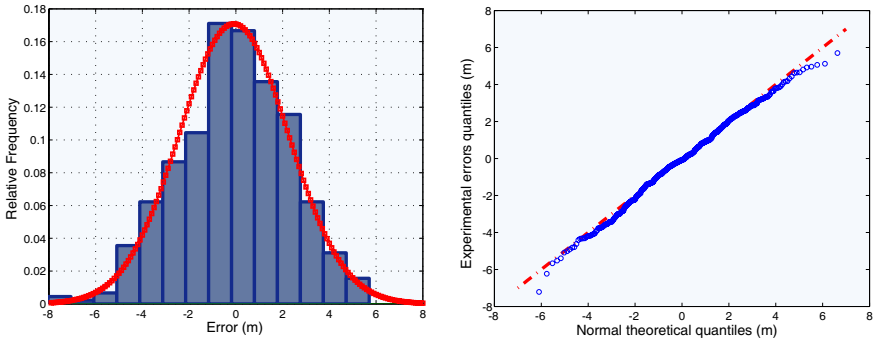

(a) LOS (b) Probability plot

Figure 4. RTT estimations distribution in LOS obeying a Gaussian distribution.

distance:

$$\widehat{d}_{ij}^{LOS} = d_i + \varepsilon_{ij}^{LOS},\ i = 1, \ldots, k;\ j = 1, \ldots, t_i. \tag{8}$$

Then, the total number of estimates is $T = \sum_{i=1}^{k} t_i$, t_i being the number of estimates at each position. As shown below, LOS error in distance estimation can be modeled as a Gaussian distribution of zero mean and standard deviation $\sigma_{\varepsilon}^{LOS}$ ($\varepsilon^{LOS} \sim N(0, \sigma_{\varepsilon}^{LOS})$). The latter will depend on the propagation channel and the measuring clock resolution. The value of $\sigma_{\varepsilon}^{LOS}$ is computed as S_{ε}^{LOS}, the sample standard deviation of the errors at all distances:

$$S_{\varepsilon}^{LOS} = \left(\frac{1}{T-1} \sum_{i=1}^{k} \sum_{j=1}^{n_i} \left(\varepsilon_{ij}^{LOS} - \overline{\varepsilon^{LOS}} \right)^2 \right)^{1/2} \tag{9}$$

Figure 4(a) provides a histogram of LOS estimation errors, superimposed with the probability density function (PDF) of a Gaussian distribution. Each treatment consists of $n_{\min}$ RTT samples, $\alpha = 0.05$ and sample error $E = 0.5$ clock cycles, as detailed in next subsection. The superimposed Gaussian curve is zero mean and has a standard deviation, $\sigma_{\varepsilon}^{LOS}$, of 2.3347 m. Thirty series of measurements at the same distances as Section 2 were carried out. How well a Gaussian distribution fits the range estimates is assessed through a probability plot. Fig. 4(b) makes clear the convenience of the proposed model since the probability plot for actual range estimates and theoretical values from a Gaussian distribution is close to the 45-degree reference line. The correlation between both data-sets is 0.9976 which means an extremely strong linear relationship. If instead of LOS errors, estimations distribution at each distance is represented ($\widehat{d}_{ij}^{LOS}$ for a given i), the mean of the Gaussian PDF curve should fit for the actual distance, d_i.

The resulting Gaussian distribution, as a model for ε^{LOS}, is the most commonly adopted in related references, considering it as the bias induced by the MPCs and a function of the system's bandwidth [15]. This simple model is used below to generalize the error when NLOS is present, and LOS value of $\sigma_{\varepsilon}^{LOS}$ will be essential to obtain an accurate estimation of the new error.

4.3. Selecting the Number of Samples

Being WS the statistical estimator to be introduced in the regression model, it is possible to dynamically infer the minimum number of samples needed to be injected. This technique will allow to minimize the traffic over the network and reducing the latency of obtaining an

MU position. Accuracy of distance estimation can be managed through the number of measurements whereby a confidence level is guaranteed. However, this number is not worth increasing indefinitely as measuring system accuracy is limited by the 44 MHz MU baseband processor clock. Hence, it is possible to minimize it until accuracy reduction is appreciated.

In case RTT measurements were Weibull distributed, the maximum likelihood estimator (MLE) of the WS ($\widehat{\eta}$) would be Gaussian with mean the WS (η) and variance the inverse of the Fisher information (i.e., $(I_n(\eta))^{-1}$) [28]. Although, in the previous section, it was shown that the RTT distribution is more complicated than the Weibull, Fig. 4 proves the Gaussian behavior of range estimates ($\widehat{\eta}$) for a sufficiently large number of samples (n). Therefore, as distance is obtained as a linear combination of the WS of RTT measurements, the distribution of $\widehat{\eta}$ is approximately Gaussian with mean η. This was proved thanks to the fact that actual measurements could be carried out by the PCB.

Moreover, in Fig. 5(a), $\widehat{\eta}$ as a function of $\sqrt{n}$ is shown for a distance of 35 m, repeating the experiment thirty times. As range estimates are Gaussian, the standard deviation of $\widehat{\eta}$, σ^{LOS}, is the standard error of the RTTs, se_{RTT}:

$$\sigma^{LOS} = se_{RTT} = \frac{\sigma_{RTT}}{\sqrt{n}} \tag{10}$$

being σ_{RTT} the standard deviation of the RTTs. In Fig. 5(a), σ^{LOS} approximately fits $\sqrt{(I_n(\eta))^{-1}}$, and by 95% of range estimates are within the curve σ^{LOS}. This result can be used to approximate se_{RTT} by $\sqrt{(I_n(\eta))^{-1}}$. Appendix A shows that Fisher information depends on WS, thus, substituting $\widehat{\eta}$ for η in the expression of $I_n(\eta)$, it is possible to compute the expected Fisher information, $I_n(\widehat{\eta})$, and hence, the estimated standard error, $\widehat{se}_{RTT}$:

$$I_n(\widehat{\eta}) = \frac{n \cdot \beta^2}{\eta^2} \tag{11}$$

where β is the shape parameter of Weibull distribution. Thus, considering (10), it is possible to define an approximate 100 $(1-\alpha)$% confidence interval (CI) for the significance level α, as:

$$\left[\widehat{\eta} - z_{1-\alpha/2} \cdot \widehat{se}_{RTT}, \widehat{\eta} - z_{1-\alpha/2} \cdot \widehat{se}_{RTT}\right] \tag{12}$$

where $z_{1-\alpha/2}$ is the point on the standard Gaussian density curve such that the probability of observing a value greater than $z_{1-\alpha/2}$ is equal to $1-\alpha/2$.

Once selected the confidence level, $1-\alpha$, and the sample error, $E = \pm z_{1-\alpha/2} \cdot \widehat{se}_{RTT}$, and under the assumptions which allow RTT

measurements to be treated as i.i.d. observations, it is straightforward to calculate the minimum number of frames needed:

$$n_{\min} \geqslant \frac{z_{1-\alpha/2}^2 \cdot \widehat{\eta}^2}{\widehat{\beta}^2 \cdot E^2} \tag{13}$$

being $\widehat{\beta}$ the observed shape parameter of Weibull distribution. This is the work carried out in the respective process of the flowchart of Fig. 1.

Figure 5(b) shows the relationship between $n_{\min}$, the sample error and the confidence level $1-\alpha$ for the RTT measurements taken from one AP inside the Higher Technical School of Telecommunications Engineering of the University of Valladolid, Spain (ETSIT-UVa). $n_{\min}$

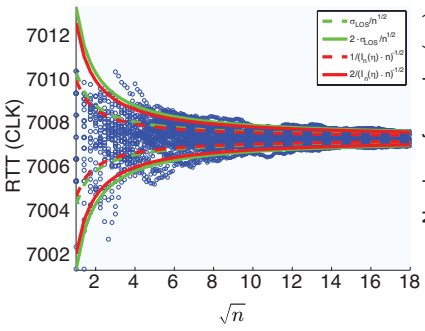

(a) $\sigma_{\varepsilon}^{LOS}$given by the Fisher information.

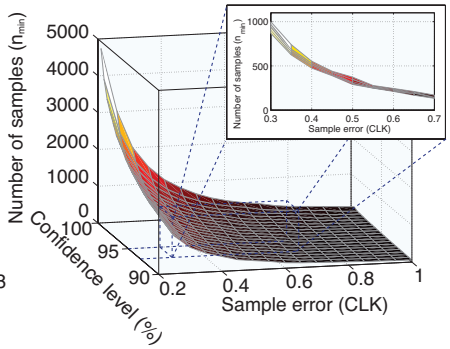

(b) n_{min} as a function of the *se* and the confidence level.

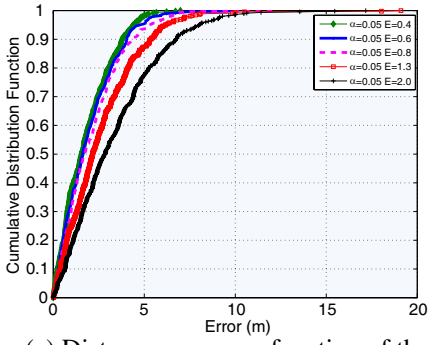

(c) Distance error as a function of the sample error.

Figure 5. The number of samples must be the smallest possible but it is limited by the distance error.

is highly influenced by sample error. However, common choices for the confidence level do not alter $n_{\min}$ significantly, increasing this number to a large extent only for values greater than 99%. Fig. 5(b) focuses on the sample error influence on $n_{\min}$ and Fig. 5(c) on its influence on range estimation error.

Other advantage of WS estimation over a traditional estimation based on the sample mean [9, 29] is the number of frames injected. Comparing the minimum number of RTT measurements needed to guarantee a given confidence level using the WS as estimator, to the one using the sample mean, for any series of RTT measurements taken with the PCB, this value is always lower for the WS, being for the sample mean:

$$n_{sample\_mean} \geqslant \frac{z_{1-\alpha/2}^2 \cdot S^2}{E^2} \tag{14}$$

where S is the sample standard deviation of the RTT measurements. Thus, as well as obtaining the most accurate range estimates, time and traffic savings are achieved with the WS parameter.

Apart from reducing positioning time and network traffic, $n_{\min}$ will affect the positioning accuracy if it is reduced too much. Fig. 5(c) depicts the cumulative distribution function (CDF) for the error in distance estimation for different values of sample error, being the confidence level 95% for all the functions. CDF was computed with $n_{\min}$ samples of the RTT LOS measurements of previous section. According to Fig. 5(c), accuracy gotten by increasing $n_{\min}$ (as a consequence of a sample error drop) is limited by the measuring system resolution. CDF for a sample error of 0.4 clock cycles almost fits with the one obtained with 0.6 cycles. Therefore, a significant level of 0.05 and a sample error of 0.5 cycles are good choices for this measuring system.

4.4. NLOS Scenario

For modeling the NLOS case, the sum of two random variables is considered as the distribution of distance estimation error. The first one is related to the LOS error, ε_{ij}^{LOS}. The second one contains NLOS estimation errors, ε_{ij}^{NLOS}. Similar to (8), in NLOS scenarios, RTT estimation can be expressed as:

$$\widehat{d}_{ij}^{NLOS} = d_i + \varepsilon_{ij}^{LOS} + \varepsilon_{ij}^{NLOS},\ i = 1, \ldots, k;\ j = 1, \ldots, t_i. \tag{15}$$

The distribution that ε^{NLOS} obeys has been analyzed in depth in the literature. Gaussian, Exponential, Weibull, and Gamma distributions are commonly proposed as NLOS error distribution [15–17]. It is known that the PDF of the sum of two random variables,

ε^{LOS} and ε^{NLOS}, is equal to the convolution of the PDFs, p^{LOS} and p^{NLOS}, of the two variables. As explained in the previous section, $\varepsilon^{LOS} \sim N(0, \sigma_{\varepsilon}^{LOS})$. Thus, in the general case, the PDF of the error in distance estimation in NLOS is:

$$\begin{aligned} p_{\varepsilon}(\widehat{d}) &= \int_{-\infty}^{\infty} p_{\varepsilon}^{NLOS}(x) \frac{1}{\sqrt{2\pi}\sigma_{\varepsilon}^{LOS}} e^{-\left(\frac{\widehat{d}-x-d}{\sqrt{2\pi}\sigma_{\varepsilon}^{LOS}}\right)^2} dx \\ &= \int_{-\infty}^{\infty} p_{\varepsilon}^{NLOS}(x) \frac{1}{\sqrt{2\pi}\sigma_{\varepsilon}^{LOS}} e^{-\left(\frac{x-(\widehat{d}-d)}{\sqrt{2\pi}\sigma_{\varepsilon}^{LOS}}\right)^2} dx \end{aligned} \tag{16}$$

therefore,

$$p_{\varepsilon}(\widehat{d}) = E\left(p_{\varepsilon}^{NLOS}(x)\right), \; x \sim N\left(\widehat{d} - d, \sigma_{\varepsilon}^{LOS}\right). \tag{17}$$

In this paper, ε^{NLOS} will be modeled as Exponentially distributed, as proposed in [15]. Particularizing (16) for $\varepsilon^{NLOS} \sim \text{Exp}(1/\lambda_{\varepsilon}^{NLOS})$, the PDF for the errors being the MU and the AP in NLOS situation is as follows:

$$p_{\varepsilon}(\widehat{d}) = c\frac{\sqrt{\pi}}{2}(1 + \text{erf}(l)) \tag{18}$$

where, as explained in Appendix B, l and c are defined as a function of $\widehat{d}$, $\sigma_{\varepsilon}^{LOS}$ and the rate parameter of the NLOS error Exponential PDF, $\lambda_{\varepsilon}^{NLOS}$.

Probably, Gamma or Weibull distribution would provide a better fit to actual NLOS errors than Exponential distribution, due to the fact that these distributions have two degrees of freedom instead of only one of the Exponential, and thus, NLOS effects can be controlled by varying more than one parameter. However, the use of the Exponential distribution is more desirable as $\lambda_{\varepsilon}^{NLOS}$ can easily be estimated from RTT measurements through the sum distribution, with known value of $\sigma_{\varepsilon}^{LOS}$, 2.3347 m. The value of $\sigma_{\varepsilon}^{LOS}$ was computed as the sample standard deviation of the errors at all distances. Computing $\lambda_{\varepsilon,i}^{NLOS}$ each time the channel changes (subindex i implies the distance), results will better fit actual samples. However, as the first approach, $0.3514\,\text{m}^{-1}$ is used as only $\lambda_{\varepsilon}^{NLOS}$ value for the indoor NLOS environment in order to treat errors at the same level of generality. In the next section, a simple method to estimate $\lambda_{\varepsilon}^{NLOS}$, through the record of measurements taken over a time window, is evaluated in order to assess the improvement of the PNMC correction method when $\lambda_{\varepsilon}^{NLOS}$ and the window size change dynamically.

Figure 6(a) shows a histogram of range estimation errors, superimposed with the convolution of Gaussian and Exponential PDFs. The number of samples taken to carry out each distance estimation is

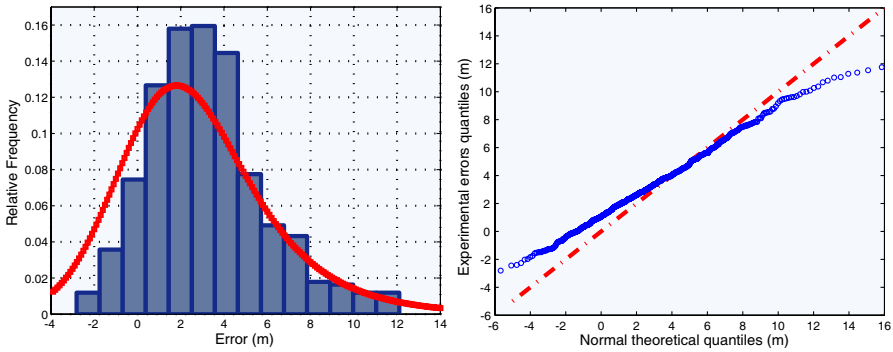

(a) NLOS (b) Probability plot

Figure 6. RTT estimations distribution in NLOS obeying the convolution of a Gaussian and an Exponential distribution.

$n_{\min}$, being $\alpha = 0.05$ and $E = 0.5$ clock cycles. The superimposed curve is the convolution of a zero mean Gaussian distribution with the value $\sigma_{\varepsilon}^{LOS}$ obtained in the previous subsection, and an Exponential distribution with $\lambda_{\varepsilon}^{NLOS}$ the described above. Again, thirty groups of measurements at the same distances as Section 2 were carried out but, in this case, MU and AP were inside the ETSIT-UVa and always in NLOS separated by a brick wall 16.4 cm width. As well as in LOS case, if instead of NLOS errors, estimations distribution at each distance is represented ($\widehat{d}_{ij}^{NLOS}$ for a given i), the mean of the Gaussian curve should fit for the actual distance.

As appreciated in Fig. 6(b), the probability plot for the experimental data and theoretical values from (18) falls approximately on a straight line, corroborated by the strong correlation (0.9952) between both data-sets. However, its intercept and slope differ slightly from the theoretical values since a single parameter is used to fit the data.

5. CORRECTING THE NLOS ERROR

Regarding the flowchart in Fig. 1, this section deals with the process *Correct NLOS* which is based on the PNMC method. In [16], the authors demonstrated a great increase in the accuracy obtained through the previous usage of the PNMC method to correct the measurements. This paper suggests a dynamic actualization of two of its input arguments: the window size and the value of $\lambda_{\varepsilon}^{NLOS}$ for the Exponential distribution. The results included in this section are

obtained from the NLOS RTT estimations regarding an AP along the route followed in [10], a 34.7 m × 19.4 m rectangle around several offices and rooms.

In LOS case, the sample standard deviation (S_ε^{LOS}) is an unbiased and efficient estimator of σ_ε^{LOS}. In order to assure that S_ε^{LOS} fits with σ_ε^{LOS}, similarly to Section 4, the minimum number of estimators, $T_{\min}$, needed to guarantee a confidence level, $1-\alpha$, can be computed. In a normally distributed population with variance σ_ε^{LOS}, sample standard deviations follow a χ^2 distribution, i.e., $\chi^2 = \frac{(T-1)S_\varepsilon^{LOS\,2}}{\sigma_\varepsilon^{LOS\,2}}$. Therefore, it is possible to define an approximate 100 $(1-\alpha)$% CI for σ_ε^{LOS} at the

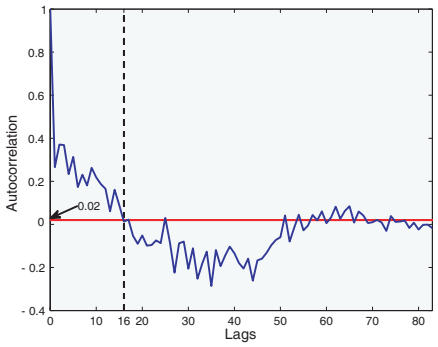

(a) Autocorrelation

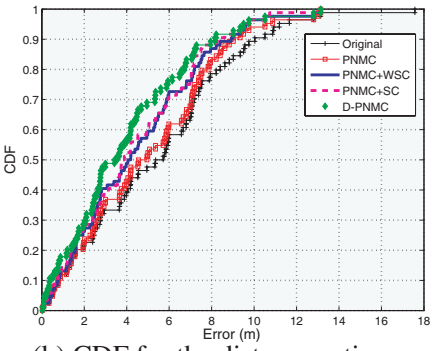

(b) CDF for the distance estimation errors

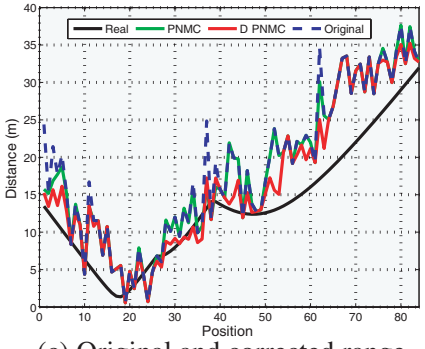

(c) Original and corrected range estimates.

Figure 7. D-PNMC computes dynamically its input parameters.

significance level α, as:

$$\left[\frac{\sqrt{T-1}\cdot S_{\varepsilon}^{LOS}}{\sqrt{\chi^2_{\alpha/2,T-1}}}, \frac{\sqrt{T-1}\cdot S_{\varepsilon}^{LOS}}{\sqrt{\chi^2_{1-\alpha/2,T-1}}}\right] \tag{19}$$

whereby $T_{\min}$ is obtained, as in previous case, once fixed a constant value for the CI.

PNMC method assumes that LOS and NLOS samples, included in distance estimation process, are independent. Thus standard deviation of sum distribution is $\sigma_{\varepsilon} = (\sigma_{\varepsilon}^{LOS\,2} + \sigma_{\varepsilon}^{NLOS\,2})^{1/2}$. As sample standard deviation is larger than in LOS case, the condition that the number of estimators, $T_{\min}$, must satisfy is more restrictive, i.e., $T_{\min}$ will be greater in the presence of NLOS. Standard deviation of an Exponential distribution fits with its mean (in this case, the inverse of $\lambda_{\varepsilon}^{NLOS}$), thus, it is straightforward to compute σ_{ε}, whereby $\lambda_{\varepsilon}^{NLOS}$ can be obtained as:

$$\lambda_{\varepsilon}^{NLOS} = \frac{1}{\sqrt{\sigma_{\varepsilon}{}^2 - \sigma_{\varepsilon}^{LOS\,2}}} \tag{20}$$

As PNMC is applied to the record of measurements over a time window, where propagation channel is similar and NLOS errors obey approximately the same distribution, $\lambda_{\varepsilon}^{NLOS}$ will be different for each one of these windows. Hence, a better correction result should be achieved if $\lambda_{\varepsilon}^{NLOS}$ is computed for each one of them. Known $\sigma_{\varepsilon}^{LOS}$ and computing σ_{ε} for the range estimates included in each time window, $\lambda_{\varepsilon}^{NLOS}$ is easily obtained, using (20), and dynamically changed each time PNMC is applied. However, the assumption of independence of NLOS estimations is not totally satisfied as drawn from a similar analysis as the one made for individual RTT measurements in [9]. In Fig. 7(a), adjacent and near-adjacent estimations show a high degree of autocorrelation probably due to the fact that in indoor environments, and for nearby positions, NLOS effects are not randomly distributed. Therefore, channel structure does not change appreciably over very short distances. This is a similar behavior to the one commented in Section 3, when obstacles which cause multipath fading are not located with complete randomness. With these estimations, the value of $\lambda_{\varepsilon}^{NLOS}$ obtained is slightly greater than the actual one, due to the dependence between the estimations. Despite this, NLOS correction will achieve a smaller error using dynamic $\lambda_{\varepsilon}^{NLOS}$ than the one obtained with a constant value.

Nevertheless, this drawback can be solved if it is utilized to identify the size of the time window where to apply PNMC and compute the corresponding $\lambda_{\varepsilon}^{NLOS}$ [30]. As new range estimates are obtained, autocorrelation among original (still not corrected) estimations is

carried out. Next, PNMC is applied to the first estimations, where autocorrelation is not near zero (in Fig. 7(a) autocorrelation exceeds 0.02 until 16th estimation), with the $\lambda_{\varepsilon}^{NLOS}$ obtained for this window using (20). Moreover, the window size must be, at least, $T_{\min}$ to guarantee Gaussian behavior of LOS errors.

This dynamic version of the PNMC correction method (D-PNMC) corrects a greater number of measurements and obtains a smaller error for those corrected by simple PNMC. This feature is observed in Fig. 7(b), where the CDF of the distance estimation error is shown for the following cases: original, static PNMC, PNMC and dynamic window size computation (PNMC+WSC), PNMC and dynamic $\lambda_{\varepsilon}^{NLOS}$ computation (PNMC+SC), and D-PNMC estimations. Moreover, in Fig. 7(c), D-PNMC estimations tend to cluster around actual distances in a more marked manner than in the simple PNMC case. In fact, the root mean square error is respectively 6.51, 5.96 and 4.98 m for original, PNMC and D-PNMC estimations.

6. CONCLUSION

In this paper, results obtained with a discrete RTT measuring system have been discussed. The work focuses on statistical behavior of RTT measurements and of the error in distance estimation, for both LOS and NLOS indoor environments.

The results have pointed out the following about the propagation channel: (1) The RTT measuring system can be modeled as a discrete time LTI system whose impulse response is determined by the MPCs present at each propagation channel. (2) The indoor propagation channel is quasi-static, varying as MU is moving. Spatial correlations govern the RTT, thus channel structure does not change appreciably over very short distances. (3) An HPP model is inadequate to describe the RTT. The distribution of the RTT measurements within a building tends to be an NHPP, and its skewness and kurtosis give information about the multipath and the distance between the MU and the AP. However, the commonly adopted Δ-K model does not work out since RTT measurements are i.i.d. (4) Errors in distance estimation obey a Gaussian distribution when MU and AP are in LOS. (5) Exponential distribution fits closely the error in distance estimation caused by the presence of NLOS measurements. The curve fittings between empirical measurements and the theoretical sum of a Gaussian and an Exponential random variables is satisfactory and, moreover, the simplest model has been selected.

Regarding the mentioned results, a dynamic computation of PNMC input arguments has been proposed to correct the NLOS error.

This method outperforms the conventional PNMC based on static values of the Exponential rate parameter and window size. The results achieved proved the goodness of this approach for positioning error minimization when locating an MU in an indoor environment.

ACKNOWLEDGMENT

This research is partially supported by the Directorate General of Telecommunications of the Regional Ministry of Public Works from Castilla y León (Spain).

APPENDIX A. MLE OF THE SCALE PARAMETER OF THE WEIBULL DISTRIBUTION

In this appendix, the scale parameter of Weibull distribution (WS) is estimated by using the MLE method and assuming that the shape parameter is known.

The probability density function of a Weibull (two parameter) random variable x is

$$\begin{aligned} f(x;\beta,\eta) &= \frac{\beta}{\eta}\left(\frac{x}{\eta}\right)^{\beta-1}\cdot e^{-\left(\frac{x}{\eta}\right)^{\beta}} \quad x \geq 0 \\ &= \frac{\beta}{\eta^{\beta}}\cdot x^{\beta-1}\cdot e^{-\left(\frac{x}{\eta}\right)^{\beta}} \quad x \geq 0 \end{aligned}$$

where $\beta > 0$ is the shape parameter and $\eta > 0$ is the WS.

Let $X_1, X_2, \ldots, X_n$ be a random sample of random variables with a two-parameter Weibull distribution, β and η. The likelihood function is

$$L_n(x_1,\ldots,x_n;\beta,\eta) = \prod_{i=1}^{n} f(x_i;\beta,\eta)$$

Therefore,

$$\begin{aligned} &\ln L_n(x_1,\ldots,x_n;\beta,\eta) \\ =\ &\sum_{i=1}^{n} \ln f(x_1,\ldots,x_n;\beta,\eta) \\ =\ &\sum_{i=1}^{n}\left(\ln\left(\frac{\beta}{\eta}\right) + (\beta-1)\cdot\ln\left(\frac{x_i}{\eta}\right) - \left(\frac{x_i}{\eta}\right)^{\beta}\right) \end{aligned}$$

$$
\begin{aligned}
&= n \cdot \ln\left(\frac{\beta}{\eta}\right) + (\beta - 1) \cdot \sum_{i=1}^{n} \ln\left(\frac{x_i}{\eta}\right) - \sum_{i=1}^{n} \left(\frac{x_i}{\eta}\right)^{\beta} \\
&= n \cdot \ln\left(\frac{\beta}{\eta}\right) + (\beta - 1) \cdot \left[-n \cdot \ln(\eta) + \sum_{i=1}^{n} \ln(x_i)\right] - \sum_{i=1}^{n} \left(\frac{x_i}{\eta}\right)^{\beta} \\
&= n \cdot \ln(\beta) + (\beta - 1) \cdot \sum_{i=1}^{n} \ln(x_i) - n \cdot \beta \cdot \ln(\eta) - \eta^{-\beta} \cdot \sum_{i=1}^{n} x_i^{\beta}
\end{aligned}
$$

thus,

$$
\frac{\partial \ln L_n}{\partial \eta} = -n \cdot \beta \cdot \frac{1}{\eta} + \beta \cdot \frac{1}{\eta^{\beta+1}} \cdot \sum_{i=1}^{n} x_i^{\beta}
$$

in order to find the maximum, $\frac{\partial ln L_n}{\partial \eta} = 0$ then,

$$
\begin{aligned}
0 &= -n \cdot \beta \cdot \frac{1}{\eta} + \beta \cdot \frac{1}{\eta^{\beta+1}} \cdot \sum_{i=1}^{n} x_i^{\beta} \\
&= \frac{\sum_{i=1}^{n} x_i^{\beta} - n \cdot \eta^{\beta}}{\eta^{\beta+1}} \\
&= \sum_{i=1}^{n} x_i^{\beta} - n \cdot \eta^{\beta}
\end{aligned}
$$

hence, the MLE of the WS

$$
\hat{\eta} = \left[\frac{1}{n} \sum_{i=1}^{n} x_i^{\beta}\right]^{\frac{1}{\beta}}
$$

this expression is known as the generalized mean or Hölder mean.

Once $\hat{\eta}$ is the MLE of η of Weibull distribution, the Fisher information ($I_n(\eta)$) and the Cramer-Rao lower bound ($I_n^{-1}(\eta)$) are computed.

The Fisher information, $I_n(\eta)$:

$$
\begin{aligned}
I_n(\eta) &= -E_\eta \left[\frac{\partial^2 \ln L}{\partial \eta^2}\right] \\
&= -E_\eta \left[-n \cdot \beta \cdot \left(-\frac{1}{\eta^2}\right) + \beta \cdot (-\beta - 1) \cdot \frac{1}{\eta^{\beta+2}} \sum_{i=1}^{n} x_i^{\beta}\right] \\
&= -\frac{n \cdot \beta}{\eta^2} + \frac{\beta \cdot (\beta + 1)}{\eta^{\beta+2}} \cdot \sum_{i=1}^{n} E_\eta(x_i^{\beta})
\end{aligned}
$$

where,

$$E_\eta(x^\beta) = \int_0^\infty x^\beta \cdot \frac{\beta}{\eta} \cdot \left(\frac{x}{\eta}\right)^{\beta-1} \cdot e^{-\left(\frac{x}{\eta}\right)^\beta} dx$$

taking $t = \left(\frac{x}{\eta}\right)^\beta$ therefore,

$$E_\eta(x^\beta) = \int_0^\infty t \cdot e^{-t} \cdot \eta^\beta dt = \eta^\beta \int_0^\infty t \cdot e^{-t} = \eta^\beta \Gamma(2) = \eta^\beta$$

Then,

$$\begin{aligned} I_n(\eta) &= -\frac{n \cdot \beta}{\eta^2} + \frac{\beta \cdot (\beta+1)}{\eta^{\beta+2}} \cdot n \cdot \eta^\beta \\ &= -\frac{n \cdot \beta}{\eta^2} + \frac{\beta \cdot (\beta+1) \cdot n}{\eta^2} \\ &= \frac{n \cdot \beta^2}{\eta^2} \end{aligned}$$

And thus, the Cramer-Rao lower bound, $I_n^{-1}(\eta)$:

$$I_n^{-1}(\eta) = \frac{\eta^2}{n \cdot \beta^2}$$

APPENDIX B. DENSITY FUNCTION OF ERRORS

Let X and Y be two independent random variables being $X \sim N(0, \sigma)$ and $Y \sim \text{Exp}(1/\lambda)$. And let Z be $Z = X + Y$. The PDFs of X and Y are respectively:

$$f(x) = \frac{1}{\sqrt{2\pi}\sigma} e^{-\frac{1}{2}\left(\frac{x}{\sigma}\right)^2}, \ (x \in R)$$

and,

$$g(x) = \lambda e^{-\lambda x}, \ (x \geqslant 0)$$

The density function of the sum of X and Y (i.e., the PDF of Z) is the convolution of $f(x)$ and $g(x)$. Thus, $h(z) = (f * g)(z)$. Therefore the PDF of Z is:

$$h(z) = \int_{-\infty}^{z} \frac{1}{\sqrt{2\pi}\sigma} e^{-\frac{1}{2}\left(\frac{x}{\sigma}\right)^2} \lambda e^{-\lambda(z-x)} dx$$

which after some manipulation simplifies to

$$h(z) = \frac{\lambda e^{-\lambda(z)} e^{\frac{(\lambda\sigma)^2}{2}}}{\sqrt{\pi}} \int_{-\infty}^{\frac{1}{\sqrt{2}\sigma} z - \frac{\lambda\sigma}{\sqrt{2}}} e^{-t^2} dt$$

Using the relationship $l = \frac{1}{\sqrt{2}\sigma} z - \frac{\lambda\sigma}{\sqrt{2}}$ and $c = \frac{1}{\sqrt{\pi}} \lambda e^{-\lambda z} e^{\frac{(\lambda\sigma)^2}{2}}$, then $h(z)$ is given by

$$h(z) = c\frac{\sqrt{\pi}}{2}(1 + \mathrm{erf}(l))$$

REFERENCES

1. Lachapelle, G., "GNSS indoor location technologies," *Journal of Global Positioning Systems*, Vol. 3, No. 1–2, 2–11, 2004.
2. Liew, S. C., K. G. Tan, and C. P. Tan, "Non-taylor series based positioning method for hybrid GPS/Cellphone system," *Journal of Electromagnetic Waves and Applications*, Vol. 20, No. 6, 717–729, 2006.
3. Liew, S. C., K. G. Tan, and T. S. Lim, "Investigation of direct A-GPS positioning for hybrid E-OTD/GNSS," *Journal of Electromagnetic Waves and Applications*, Vol. 20, No. 1, 79–87, 2006.
4. Tan, K. G., A. R. Wasif, and C. P. Tan, "Objects tracking utilizing square grid rfid reader antenna network," *Journal of Electromagnetic Waves and Applications*, Vol. 22, No. 1, 27–38, 2008.
5. Tayebi, A., J. Gómez, F. Saez de Adana, and O. Gutierrez, "The application of ray-tracing to mobile localization using the direction of arrival and received signal strength in multipath indoor environments," *Progress In Electromagnetics Research*, PIER 91, 1–15, 2009.
6. Soliman, M. S., T. Morimoto, and Z. I. Kawasaki, "Three-dimensional localization system for impulsive noise sources using ultra-wideband digital interferometer technique," *Journal of Electromagnetic Waves and Applications*, Vol. 20, No. 4, 515–530, 2006.
7. Seow, C. K. and S. Y. Tan, "Localization of omni-directional mobile device in multipath environments," *Progress In Electromagnetics Research*, PIER 85, 323–348, 2008.
8. Yarkony, N. and N. Blaunstein, "Prediction of propagation characteristics in indoor radio communication environment," *Progress In Electromagnetics Research*, PIER 59, 151–174, 2006.
9. Prieto, J., A. Bahillo, S. Mazuelas, J. Blas, P. Fernández, and R. M. Lorenzo, "RTS/CTS mechanism with IEEE 802.11 for indoor location," *Proceedings of the NAV08/ILA37, The Navigation Conference and Exhibition*, London, October 2008.

10. Prieto, J., A. Bahillo, S. Mazuelas, R. M. Lorenzo, J. Blas, and P. Fernández, "Adding indoor location capabilities to an IEEE 802.11 wlan using real-time RTT measurements," *Proceedings of the IEEE Wireless Telecommunications Symposium*, Prague, April 2009.
11. Zhang, W., "Physical modeling of wide-band propagation for urban line-of-sight mirco-cellular mobile and personal communications," *Journal of Electromagnetic Waves and Applications*, Vol. 11, No. 12, 1633–1648, 1997.
12. Blas Prieto, J., P. Fernández Reguero, R. M. Lorenzo Toledo, E. J. Abril, S. Mazuelas Franco, A. Bahillo Martinez, and D. Bullid, "A model for transition between outdoor and indoor propagation," *Progress In Electromagnetics Research*, PIER 85, 147–167, 2008.
13. Turin, G. L., F. D. Clapp, T. L. Johnston, S. B. Fine, and D. Lavry, "A statistical model of urban multipath propagation," *IEEE Transactions on Vehicular Technology*, Vol. 21, No. 1, 1–9, 1972.
14. Boutin, M., A. Benzakour, C. L. Despins, and S. Affes, "Radio wave characterization and modeling in underground mine tunnels," *IEEE Transactions on Antennas and Propagation*, Vol. 56, No. 2, 540–549, 2008.
15. Alsindi, N., B. Alavi, and K. Pahlavan, "Measurement and modeling of ultra wideband toa-based ranging in indoor multipath environments," *IEEE Transactions on Vehicular Technology*, Vol. 58, No. 3, 1046–1058, 2009.
16. Mazuelas, S., F. A. Lago, J. Blas, A. Bahillo, P. Fernández, R. M. Lorenzo, and E. J. Abril, "Prior NLOS measurements correction for positioning in cellular wireless networks," *IEEE Transactions on Vehicular Technology*, Vol. 58, No. 5, 2585–2591, 2009.
17. Qi, Y., H. Kobayashi, and H. Suda, "On time-of-arrival positioning in a multipath environment," *IEEE Transactions on Vehicular Technology*, Vol. 55, No. 5, 1516–1526, 2006.
18. Chen, V. C. and H. Ling, *Time-frequency Transforms for Radar Imaging and Signal Analysis*, Artech House, Norwood, 2002.
19. Bahillo, A., J. Prieto, S. Mazuelas, R. M. Lorenzo, J. Blas, and P. Fernández, "IEEE 802.11 distance estimation based on RTS/CTS two-frame exchange mechanism," *Proceedings of the IEEE Transactions on Vehicular Technology Conference*, Barcelona, April 2009.
20. Mak, L. C. and T. Furukawa, "A time-of-arrival-based positioning

technique with non-line-of-sight mitigation using low-frequency sound," *Journal of Electromagnetic Waves and Applications*, Vol. 22, No. 5, 507–526, 2008.

21. Güvenç, I., C.-C. Chong, F. Watanabe, and H. Inamura, "NLOS identification and weighted lest-squares localization for UWB systems using multipath channel statistics," *EURASIP Journal on Advances in Signal Processing*, Vol. 2008, DOI: 10.1155/2008/271984, 2008.
22. Suzuki, H., "A statistical model for urban radio propagation," *IEEE Transactions on Communications*, Vol. 25, No. 7, 673–680, 1977.
23. Hashemi, H., "The indoor radio propagation channel," *Proceedings of the IEEE*, Vol. 81, No. 7, 943–968, 1993.
24. Saleh, A. and R. Valenzuela, "A statistical model for indoor multipath propagation," *IEEE Journal on Selected Areas in Communications*, Vol. 5, No. 2, 128–137, 1987.
25. Takamizawa, H., S. Seidel, and T. Rappaport, "Indoor radio channels models for manufacturing environments," *Proceedings of the IEEE Southeastcon '89, Energy and Information Technologies in the Southeast*, Vol. 2, 750–754, April 1989.
26. Arkin, B. L. and L. M. Leemis, "Nonparametric estimation of the cumulative intensity function for a nonhomogeneous poisson process from overlapping realizations," *Management Science*, Vol. 46, No. 7, 989–998, July 2000.
27. Hocking, R. R., "Regression on functions of one variable," *Methods and Applications of Linear Models: Regression and the Analysis of Variance*, Wiley, New Jersey, 2003.
28. Knight, K., *Mathematical Statistics*, Chapman & Hall/CRC, Boca Raton, 1999.
29. Ciurana, M., F. Barcelo-Arroyo, and F. Izquierdo, "A ranging system with IEEE 802.11 data frames," *Proceedings of the IEEE Radio Wireless Symposium Conference*, 133–136, January 2007.
30. Box, G., *Time Series Analysis: Forecasting and Control*, Wiley, New York, 1994.